Journal of
Applied Crystallography

ISSN 0021-8898

Received 13 May 2008
Accepted 17 September 2008

DuMond analysis of bending in single crystals by Laue diffraction using σ–π polarization geometry

Jorge Serrano,[a,b]* Claudio Ferrero,[b] Marco Servidori,[c] Jürgen Härtwig[b] and Michael Krisch[b]

[a]ICREA and Departmento de Fisica Aplicada, EPSC, Universitat Politècnica de Catalunya, Avenida Canal Olimpic 15, 08860 Castelldefels, Spain, [b]European Synchrotron Radiation Facility, BP 220, 38043 Grenoble, France, and [c]CNR–IMM, Via Gobetti 101, 40129 Bologna, Italy. Correspondence e-mail: jserrano@fa.upc.edu

A DuMond analysis of X-ray diffraction patterns has been carried out in the case of a combined σ–π polarization configuration, obtained using a setup with a double-crystal monochromator in reflection (Bragg) geometry and an analyser in transmission (Laue) geometry. The derived analytical expressions allow the characterization of the bending of the analyser and the quantitative estimation of the curvature radius and its sign from the width of the crystal rocking curves. The theoretical analysis is applied to the case of a thin, accidentally bent, Si crystal.

1. Introduction

Bending of perfect crystals affects the quality of X-ray optical setups and causes changes in the observed angular widths of the crystal Bragg reflections. These circumstances may also be used to control the required divergence in beamline designs and the crystal quality needed in the preparation of monochromators. Graphical analysis *via* DuMond (1937) diagrams has proven to be a reliable method to characterize the widths of rocking curves in multi-crystal systems arranged in both σ–σ and, in particular, the less commonly used σ–π X-ray polarization configurations (Servidori *et al.*, 2001*a*). In the case of Bragg geometry, DuMond analysis has been extensively applied to both flat and curved crystals (Servidori *et al.*, 2001*a*,*b*). However, no derivation has been reported, to our best knowledge, for the case of Laue (transmission) geometry in a setup involving both σ and π polarization. This case was considered by Matsouli *et al.* (2000), but no formalism aiming to achieve a quantitative analysis was drawn.

In particular, for single crystals with a thickness of several tens of micrometres, *i.e.* mechanically thin crystals, the reflection properties in this geometry critically depend on thickness, and even slight bending is expected to lead to a departure of the width of the rocking curve from that of the perfect crystal (Uschmann *et al.*, 1993). The analytical description of the Laue case, particularly in the σ–π polarization configuration, is by no means trivial within the framework of dynamical theory. However, DuMond analysis provides a simple and reliable way to quantify the contributions, stemming from a crystal deformation, to the linewidths of different reflections as a function of the specific features of the beam.

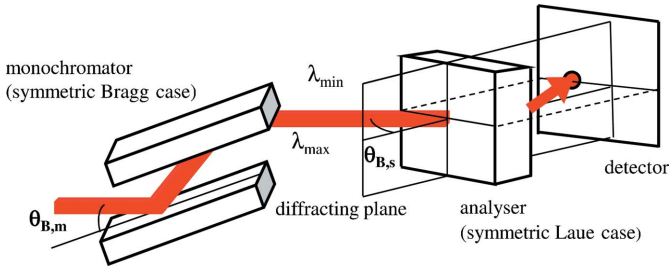

Figure 1
Scheme of the experimental setup, consisting of a double-crystal monochromator, a single-crystal analyser at the sample position and an area detector to measure the intensity of the diffracted beam.

2. DuMond analysis for a multi-crystal Bragg–Laue setup

The experimental setup corresponding to the case study of this investigation is depicted in Fig. 1. It consists of a double-crystal monochromator operating in the vertical plane together with a single-crystal analyser that diffracts the X-rays in transmission geometry in the horizontal plane. The analyser is placed at the sample position and will be referred to hereafter as the sample. The general case of a curved sample in Bragg geometry has been extensively discussed by Servidori *et al.* (2001*b*). Let us denote with the subscripts m and s the quantities referring to monochromator and sample, respectively. Let φ_m and $\delta\theta_m$ be the angular beam divergence in the plane normal and parallel, respectively, to the diffraction plane of the monochromator. They correspond to the full width at half-maximum (FWHM) of the horizontal and vertical beam profiles and are alternatively denoted by s'_y and s'_z in the literature, respectively. For the sake of comparison with the DuMond analysis of the Bragg geometry given by Servidori *et al.* (2001*b*), we shall use a similar notation here.[1] The relevant

[1] Note that Servidori *et al.* (2001*b*) considered the beam divergence half-width at half-maximum, labelled φ and $\Delta\theta$. We shall reserve the label $\Delta\theta_B$ for the deviation from the kinematical Bragg angle θ_B.

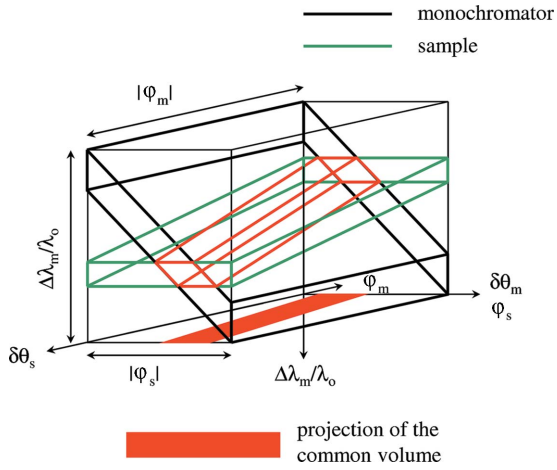

Figure 2
DuMond diagram for the σ–π geometry, showing the common diffraction volume identified by the intersection of the diffraction domains of monochromator and sample. The diagram is drawn for the sample entrance surface. The projection of the common volume onto the $\varphi_s\delta\theta_s$ plane determines the shape of the sample image.

expressions to calculate the FWHM of a sample diffraction profile result from the projection onto the $\varphi_m\delta\theta_m$ plane of the common diffraction volume determined by the intersection of the diffraction domains of monochromator and sample, shown in Fig. 2. These expressions adapted to a sample in Laue geometry become

$$l_{||} = \frac{\omega_{s,\pi}\tan\theta_{B,m} + \omega_m\tan\theta_{B,s}}{(1-\kappa)\tan\theta_{B,m}} \quad (1)$$

for the angular dimension of the red band in Fig. 3(*a*) parallel to φ_m and

$$\alpha = \arctan\left[\frac{\cos\theta_{B,s}(1-\kappa)\tan\theta_{B,m}}{\tan\theta_{B,s}}\right] \quad (2)$$

for the inclination angle of this band with respect to φ_m (Fig. 3*b*), where θ_B is the Bragg angle. The projection onto the vertical plane of the illuminated area of the sample is given by $w \times h$ (horizontal $\times$ vertical) in Fig. 3(*b*) and corresponds to the intersection of the beam divergence (FWHM) with the sample, *i.e.* in the absence of the monochromator. The term κ is given, in the Laue case, by

$$\kappa = (L/R)\cos\theta_{B,s}, \quad (3)$$

L and R being the source-to-sample distance and the sample curvature radius, positive or negative in the case of concavity or convexity, respectively, *i.e.* $\kappa = 0$ for a flat sample. Note that, in the Bragg case, a sinusoidal function replaces $\cos\theta_{B,s}$ in the definition of κ. The Darwin FWHM ω_m ($\omega_{s,\pi}$) of the intrinsic σ-polarized (π-polarized) diffraction profile of the monochromator (sample) is found to be, in the symmetric case (Zachariasen, 1945),

$$\omega_{Darwin} = 2|\Psi_H|C/\sin(2\theta_B), \quad (4)$$

where C is the polarization factor: $C = 1$ for σ polarization and $C = |\cos 2\theta_B|$ for π polarization. In the asymmetric case, the previous equations remain valid and one needs only to

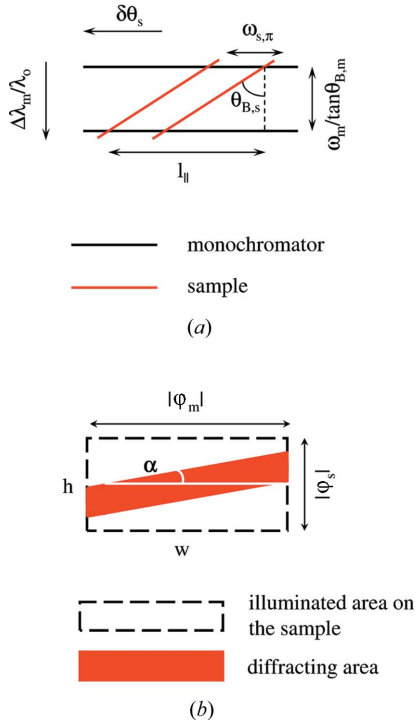

Figure 3
(*a*) Section of the diagram of Fig. 2 with a constant-φ_s plane, and (*b*) illuminated and diffracting areas of the sample for (Laue) transmission geometry.

employ the generalized expression for the Darwin width, *i.e.* with a factor $b^{1/2}$ in the denominator of equation (4), where b is the so-called asymmetry factor.[2] ω_m can be directly calculated in the symmetric Bragg case as the σ-polarized angular width in the range from $y_m = -1$ to $y_m = 1$, where

$$y_m = \frac{\Psi'_{0,m} + \Delta\theta_{B,m}\sin(2\theta_{B,m})}{|\Psi'_{H,m}|} \quad (5)$$

is the dynamical incidence parameter {see equation [3.181] of Zachariasen (1945)}. In (5), $\Psi'_{0,m}$ and $\Psi'_{H,m}$ are the real parts of the Fourier coefficients of zeroth and H order, respectively, of 4π times the crystal polarizability (Ψ_H), and $\Delta\theta_{B,m}$ is the deviation from the kinematical Bragg angle $\theta_{B,m}$. $\omega_{s,\pi}$ is obtained similarly to ω_m from the intensity profile of the Hth Bragg reflection, for which the following approximated expression of the more exact equation [3.185] of Zachariasen (1945) was used:

$$\frac{I_H}{I_0} = \frac{\exp(-\mu_0 t_0/\gamma_0)}{2(1+y_{s,\pi})}\left[1 + 2\frac{(k_s A_{s,\pi})^2}{1+y_{s,\pi}}\right]. \quad (6)$$

In equation (6), I_H and I_0 are the diffracted and incident beam intensities, respectively, μ_0 is the linear absorption coefficient, t_0 is the sample thickness, γ_0 is the direction cosine of the incident wavevector with respect to the inward normal to the

[2] Note that the Darwin width can be modified by a cylindrical bending if the cylindrical axis has a nonzero projection normal to the diffraction plane. However, this effect will not be considered in this work.

Table 1
Crystal sample parameters for $\lambda_0 = 0.15638$ nm.

Reflection	$\theta_{B,m}$ (°)	$\theta_{B,s}$ (°)	ω_m (arc s)	$\omega_{s,\pi}$ (arc s)	A	kA
111	14.44	14.44	7.05	5.73	9.8	0.31
220	14.44	24.03	7.05	3.23	9.1	0.35

Table 2
FWHMs and curvature radii calculated using the parameters from Table 1.

Sample reflection	$l_{\|\|}$ (arc s)	α (°)	R (m)	$FWHM_{calc}$ (arc s)	$FWHM_{exp}$ (arc s)
111	12.78	44.08	∞	15.21	16.7 (2)
111	14.52	40.44	407.70	16.70	16.7 (2)
220	15.44	27.81	∞	17.51	15.90 (14)
220	13.59	30.93	−339.05	15.90	15.90 (14)

entrance surface of the sample, $k_s = \Psi''_{H,s}/\Psi'_{H,s}$, where $\Psi''_{H,s}$ is the imaginary part of Ψ_H for the sample, and

$$A_{s,\pi} = \frac{\pi|\cos(2\theta_{B,s})||\Psi'_{H,s}|t_0}{\lambda(\sin\theta_{B,s}\cos\theta_{B,s})^{1/2}} \quad \text{and} \quad y_{s,\pi} = \frac{\Delta\theta_{B,s}\sin(2\theta_{B,s})}{|\Psi'_{H,s}||\cos(2\theta_{B,s})|} \tag{7}$$

are the dimensionless sample thickness and the dynamical incidence parameter, respectively, for the π-polarized symmetric Laue case.

The approximation leading to equation (6) holds for $A >> 1$, *i.e.* thick crystals in the sense of diffraction theory, and $|k|A < 0.4$. Equation (6) was used under the assumption that energy fluctuations and small thickness variations average out reflectivity interference fringes if they are narrow enough ($A >> 1$), which often happens in the real physical case. It follows that the interference thickness fringes, typical of a theoretical Laue case diffraction profile, do not appear, thus enabling a much easier determination of a well defined FWHM. In σ–π geometry, a sample rotation with respect to the monochromator implies a shift of the inclined red band in Fig. 2 parallel to $|\varphi_m|$. As to $|\varphi_m|$, we recall that the divergence of the beam normal to the diffraction plane of the monochromator at the source exit, typically with a Gaussian profile, does not change after diffraction from the monochromator. Hence, approximating $l_{||}$ to the FWHM of a Gaussian profile, the FWHMs of the sample diffraction profiles ($FWHM_{calc}$) are easily obtained as $FWHM_{calc} = (l_{||}^2 + \varphi_m^2)^{1/2}$.

3. Experimental application

In order to apply the proposed framework, we took as a sample a piece of a silicon single-crystalline wafer thinned to a thickness of 60 µm. The wafer had the surface oriented perpendicular to the $[1\bar{1}0]$ direction, which allowed us the measurement of the 111 and 220 diffraction profiles in symmetric Laue geometry. The sample was mounted on an aluminium holder featuring two contact regions. The experiment was performed on beamline ID16 of the European Synchrotron Radiation Facility (ESRF) in Grenoble, France. A double Si(111) crystal monochromator was employed to obtain monochromatic X-rays of 7.908 keV, which were diffracted by the sample and then collected by a silicon-diode detector following the scheme displayed in Fig. 1. The beam size at the sample position was 2.0 × 1.1 mm (horizontal × vertical), and the beam divergence was 40 × 22 µrad (8.25 × 4.54 arc seconds) in the horizontal × vertical directions. The distance between the source and the sample was $L = 50.45$ m.

Table 1 shows the values of A and $|k|A$ along with the Bragg angles of the 111 and 220 reflections, the Darwin width of the monochromator (ω_m), and those of the sample reflections ($\omega_{s,\pi}$). As can be noticed from Table 1, from the viewpoint of the dynamical theory of X-ray diffraction, the sample used in our measurement cannot be deemed to be thin. It hence fulfills the conditions for applying equation (6) and the above-discussed DuMond analysis. We obtained experimental diffraction profiles of 16.7 (2) and 15.90 (14) arc seconds FWHM for the 111 and 220 reflections, respectively. Notice that in Table 2, for a flat sample ($R = \infty$), neither the FWHM of the 111 reflection nor that of the 220 reflection matches the experimental value within its uncertainty, indicating that the wafer is curved. The curvature radii obtained from equations (1)–(3) that reproduce the $FWHM_{exp}$ values are also reported in Table 2. The increase (decrease) of $FWHM_{exp}$ for 111 (220) as referred to the calculated FWHM for a flat crystal ($FWHM_{calc}$ for $R = \infty$) is the result of the decrease (increase) of the inclination angle α (see Fig. 3*b*). On the basis of the above results it is reasonable to argue that the sample experienced some bending across the beam footprint, owing to the clamping in the sample holder. Clamping may induce quasi-cylindrical deformations, characterized by an average curvature radius, or even saddle-like distortions, with two curvature radii of opposite sign (surfaces featuring both convexity and concavity, the so-called anticlastic bending). Fig. 4 exemplifies the behaviour of the calculated FWHM *versus* the curvature radius R for the 220 reflection.

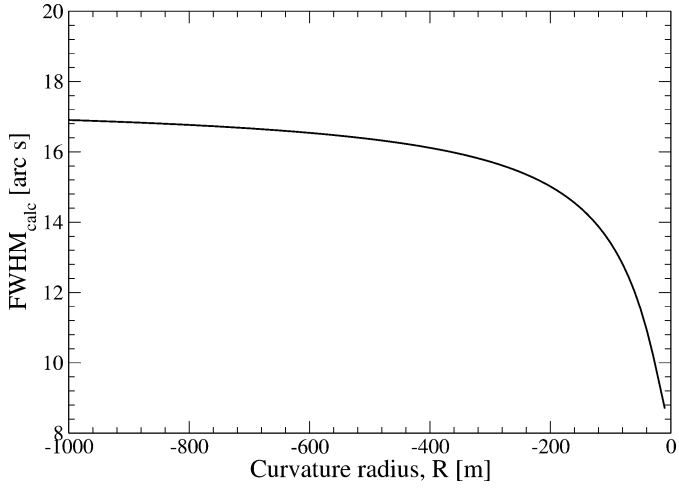

Figure 4
FWHM of the 220 reflection *versus* the curvature radius. The experimental parameters of the X-ray source of the ID16 beamline at the ESRF were employed in the calculation.

4. Conclusions

The analysis method based on the three-dimensional DuMond diagram in combined σ–π polarization proved itself highly sensitive to very small analyser deformations. The main advantage of using the σ–π setting instead of the σ–σ configuration is that the sample bending in σ–σ always causes an increase of the FWHM rocking curve, regardless of the curvature sign. As has been shown here, this does not occur in σ–π geometry. Hence, the latter allows one to distinguish between concavity and convexity *via* an increase or decrease of the FWHM and/or the clockwise or anticlockwise deviation of the inclination angle α of the diffracting area of the sample/analyser (Servidori *et al.*, 2001*b*). Therefore, saddle-like distortions of the sample can only be detected using the σ–π combination. Moreover, the σ–π combination is commonly used for inelastic X-ray scattering (IXS) experiments at synchrotron radiation sources, where the scanning double-crystal monochromator operates in the vertical scattering plane and the IXS spectrometer (the analyser) in the horizontal plane.

It should be considered that, if images are taken of the beam diffracted by the sample in addition to the measurements of the diffracted beam profile, the sample curvature can be determined by two independent parameters, *i.e.* the inclination angle α and the FWHM of the sample's rocking curve (denoted in the text as $l_{||}$). This ensures higher reliability in the measurement of the sample bending, as compared with the σ–σ setup.

Actually, differences of a few degrees in α reveal rather large curvature radii. The proposed DuMond framework hence enables one to verify promptly the expected FWHM of the rocking curve of a crystal analyser in Laue geometry with a high degree of accuracy.

Summarizing, the versatility of the method allows one to determine whether supposedly flat Laue crystals kept in sample holders are actually flat or rather feature some bending accidentally induced by the sample holder. In particular, it is possible to determine quantitatively the radius of curvature of the induced bending and its sign for any desired reflection.

We gratefully acknowledge G. Monaco, S. Huotari and F. Cembali for fruitful discussions. JS acknowledges financial support from CICYT grants MAT2007-60087 and ENE2008-04373 and Generalitat de Catalunya grants 2005SGR00535 and 2005SGR00201.

References

DuMond, J. W. M. (1937). *Phys. Rev.* **15**, 872–883.
Matsouli, I., Kvardakov, V. V. & Baruchel, J. (2000). *J. Appl. Cryst.* **33**, 1051–1058.
Servidori, M., Cembali, F. & Milita, S. (2001*a*). *Appl. Phys. A*, **73**, 75–82.
Servidori, M., Cembali, F. & Milita, S. (2001*b*). *Appl. Phys. A*, **73**, 83–90.
Uschmann, I., Förster, E., Gäbel, K., Hölzer, G. & Ensslen, M. (1993). *J. Appl. Cryst.* **26**, 405–412.
Zachariasen, W. H. (1945). *Theory of X-ray Diffraction in Crystals*, 2004 edition. Mineola: Dover Publications Inc.